A Machine Learning Degradation Model for Electrochemical Capacitors Operated at High Temperature

DARIUS ROMAN[ID][1], **SAURABH SAXENA**[ID][2], **JENS BRUNS**[ID][3], **ROBU VALENTIN**[ID][1,5], **MICHAEL PECHT**[ID][4], **(Life Fellow, IEEE), AND DAVID FLYNN**[ID][1], **(Member, IEEE)**

[1]Smart Systems Group (SSG), School of Engineering and Physical Science (EPS), Heriot-Watt University, Edinburgh EH14 4AS, U.K.
[2]Argonne National Laboratory, Lemont, IL 60439, USA
[3]Drilling Service, Baker Hughes, 29221 Celle, Germany
[4]Center for Advanced Life Cycle Engineering (CALCE), University of Maryland, College Park, MD 20742, USA
[5]Centrum Wiskunde & Informatica (CWI), 1098 Amsterdam, The Netherlands

Corresponding author: Darius Roman (dvr1@hw.ac.uk)

ABSTRACT Electrochemical capacitors (ECs) have only recently been considered as an alternative power source for telemetry sensors of drilling equipment for geothermal or oil and gas exploration. The lifecycle analysis and modelling of ECs is underrepresented in literature in comparison to other storage devices e.g. Li-ion batteries. This paper investigates the degradation of ECs when cycled outside the manufacturer-specified operating temperature envelope and proposes a machine learning-based approach for modelling the degradation. Experimental results show that end of life, defined as a 30% decrease in capacitance, occurs at 1,000 cycles when the environmental temperature exceeds the maximum operating temperature by 30%. The life-cycle test data is then used as an input to a Gaussian process regression (GPR) algorithm to predict the capacitance fade trend. The GPR is validated on a total of nine commercial cells from two different manufacturers, achieving an average root mean squared percent error of less than 2% and a mean calibration score of 93% when referenced to a 95% confidence interval. The model can be utilized to determine the EC degradation rate at a range of operating temperature values.

INDEX TERMS Machine learning, energy storage, electrochemical capacitors, supercapacitors, data analysis.

I. INTRODUCTION

Energy storage technologies represent an approximately $59 billion market that is projected to grow by $546 billion in annual revenue by 2035 [1]. Global decarbonisation of energy and transport infrastructure—utilising intermittent renewable energy generation—is driving significant growth in demand for more reliable energy storage devices [2], [3]. In parallel to this, there are also increasing demands on energy storage performance within traditional markets, such as consumer electronics, in which power density and lifetime are key metrics to product value [4]. Energy storage technologies are critical in achieving the decarbonisation goals set in line with the Paris Agreement's 2050 agenda [5]. This requires

raising the renewable energy share of the world's primary energy supply by a total of 40% from 15% in 2017 to 65% by 2050 [6]. While the global health crisis and oil price slump may suppress emissions in 2020, a rebound would restore the long-term trend [7]. In the context of energy storage, in this paper we focus on electrical energy storage, and more specifically on electrochemical capacitors (ECs). In comparison to a battery, ECs, also known as *supercapacitor*, *ultracapacitor*, or *electrochemical double-layer capacitor*, can withstand high discharge-charge currents and thus are suitable for withstanding peak power demands. An EC's long cycle life when operated in a high-temperature environment makes it ideal for applications such as oil and gas drilling [8] and space exploration [9], [10].

Within such high-value and safety-critical applications, it is vital to understand the effect of temperature on an

The associate editor coordinating the review of this manuscript and approving it for publication was Yunjie Yang[ID].

EC's cycle life expectancy. Therefore, in this work we focus on energy storage devices operated at temperatures of up to 200° C, specifically the operation of EC onboard downhole drilling equipment for geothermal or oil and gas exploration. Downhole tools are complex electromechanical systems that perform critical functions in drilling operations [11] and are capable of withstanding extreme temperatures, shocks, and vibrations.

An EC's loss of cycling ability with ageing is attributed to a fade in capacitance and an increase in equivalent series resistance (ESR). The two predominant factors that cause ageing are an increased end of charge voltage [12] and temperature [13]. Ishimoto *et al.* [12] investigated degradation by increasing operating voltage. The work concluded that the main failure modes are undesired faradaic processes that lead to capacitance fade. At high-temperature operation, the predominant failure mode was reported as electrolyte vaporization. When operated at high temperatures, an aqueous-based electrolyte can suffer from water decomposition (oxygen/hydrogen evolution), causing pressure buildup within the cell and ultimately leading to catastrophic failure, rupturing the capacitor cell [13], [14]. EC degradation trend is a complex interplay between operating condition effect (charge/discharge current), environmental temperature effects and EC material composition [15], [16], thus, predicting EC degradation, particularly when operated at high temperatures remains challenging.

Several efforts have been made to model capacitor degradation under both temperature and voltage conditions [12], [14], [17]–[19]; however, most rely on simplified exponential models that do not translate well from one manufacturer to another. Given the variability in manufactured components and application-specific direct and indirect loading, this is a limiting factor in the applicability of the current state-of-the-art models.

Machine learning has emerged as a robust method capable of accurate data analysis and generalisation outside the training population [11]. Some machine learning models can be overtuned to specific data sets, resulting in their optimal performance only occurring on constrained data sets [20]. Machine learning has seen limited application in EC degradation prediction, with most work concentrated on predicting remaining useful life [21]–[23]. Lithium-ion batteries, on the other hand, have seen extensive research in degradation prediction via machine learning modelling and therefore some of the methods proposed [24]–[27] can also be employed for EC degradation. In particular, the work of Richardson *et al.* [24] used a Gaussian process regression algorithm to forecast capacity degradation as a function of time. The authors in [24] use a GPR model with compound kernel functions in combination with a battery degradation, exponential-based parametric model and predict both short-term and long-term degradation trends. Despite the method achieving good accuracy, the method is validated on a single temperature profile rarely encountered in practice. The work of Liu *et al.* [25] combines a recurrent neural network with a GPR to predict the remaining useful life of the cell. The method first decomposes the battery capacity degradation curve using the empirical mode decomposition (EMD) and then feeds the decomposed signal to both the LSTM submodel to capture the long-term dependence, and the GPR submodel to generate the uncertainty of each prediction result. One shortcoming of the work, however, is the limited cycle data available that does not include prediction past the knee-point, a problem often encountered in real-life applications [28].

In this work, we deploy a machine learning algorithm to predict degradation trends for electrochemical double-layer capacitors beyond the knee-point onset when cycled at high temperature in an oil and gas drilling environment. Operation at high temperature accelerates EC degradation as shown in [17], we therefore investigate the worst-case scenario for the mentioned application. This paper considers samples from two manufacturers with different ratings, as opposed to previous methods [18], [19], which concentrate on a single manufacturer. We use capacitance rather than ESR as a proxy for degradation. The choice of capacitance as a state of health indicator is motivated by capacitor cells reaching the end of life (EoL) criteria—measured as a 30% decrease in capacitance—first, as opposed to ESR-based criteria of a 100% increase in resistance [17]. The modelling stage employs a Gaussian process algorithm that is fitted on two covariates (temperature and end of charge voltage) as well as two measurands (nominal capacitance value and cycle number) to predict the capacitance degradation as a function of cycle number. The GPR is selected due to its non-parametric Bayesian formulation and ability of reasoning under uncertainty quantified through the estimation of standard deviation associated with each prediction. The algorithm is trained on five samples and validated on the remaining four samples, showcasing the model's ability to generalise irrespective of rated capacity and manufacturer. In comparison to previous papers in EC modelling, [18]–[23], which include mathematical exponential models with limited assessments of prediction uncertainty, we quantify uncertainty in the prediction via confidence intervals (CIs). Uncertainty in the prediction is then assessed based on the calibration score calculated at a 95% CI, $CS_{2\sigma}$. Based on its $CS_{2\sigma}$ score, the model is then recalibrated using kernel ridge regression [29] for a more robust uncertainty estimation. The contribution of this work includes: (1) a single machine learning model capable of predicting EC degradation trend irrespective of operational temperature, (2) elimination of the need for pre-determined parametric EC degradation model by simply using temperature, nominal capacitance and end-of discharge voltage as inputs (3) model generalisation on different EC designs, (4) model ability of quantifying uncertainty in its prediction and (5) model recalibration for robust uncertainty estimation.

The paper is organised as follows. Section II - *Electrochemical capacitor overview* outlines the configuration of the EC structure, discusses sample materials analysis, and summarises manufacturer-supplied information.

Section III - *Experimental design* provides a detailed description of the experimental procedure, subsequently summarising the accelerated life-cycle test results. Section IV - *Degradation modelling* introduces the EC degradation as a machine learning regression problem and provides the mathematical framework of the Gaussian process algorithm. The section concludes with kernel choice, hyperparameter tuning strategies, and recalibration strategies. Section V - *Results* discusses algorithm input, accuracy metrics, and model calibration assessment metrics. The section concludes with an assessment of the model on test data from both an accuracy and an uncertainty point of view. Section VI - *Discussions* provides a perspective on the practical application of the method. The paper concludes with the primary findings and possible future work in Section VII – *Conclusion*.

II. ELECTROCHEMICAL CAPACITOR OVERVIEW

The double-layer EC is typically made out of two porous electrode structures, a conductive electrolyte and a separator, as illustrated in Figure 1. Despite the similar structure of the two analysed EC models, the type, composition, and concentration of the electrolyte is as important as the electrode materials, particularly for EC performance under high-temperature conditions [30]. The ECs used in this study include four samples manufactured by FastCap (model EE150-35) and five samples manufactured by LS Mtron (model LSUC 002R8S). Cyclic data for the LS Mtron samples has been imported from [17], and thus LS Mtron samples have not been tested for this work. Table 1 summarises manufacturer-indicated electrical properties and rated performance.
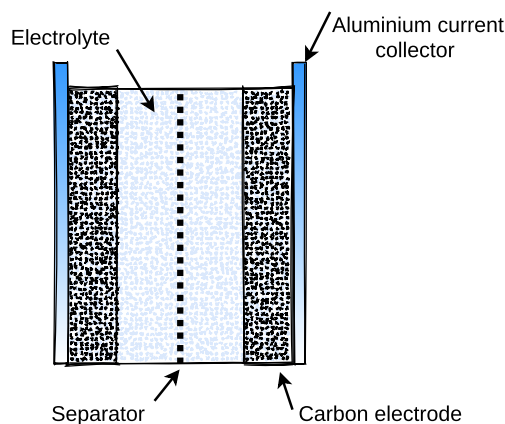

FIGURE 1. Schematic illustration of a supercapacitor.

Cell voltage is highly dependent on the electrolyte used [30], [31]. Therefore, given the ionic-based electrolyte, the FastCap EC has a maximum rated voltage of 1V. It can also be operated at a higher temperature, unlike the LS Mtron EC's organic-based electrolyte [31]. The LS Mtron samples have been previously studied by Williard *et al.* [17] and therefore are not discussed in great detail here. In summary, the LS Mtron structure consists of two activated carbon electrodes,

TABLE 1. Electrochemical capacitor properties and manufacturer rated performance.

Specification	FastCap	LS Mtron
Rated Voltage [V]	1.0	2.8
Maximum Current [A]	74.0	46.3
Surge Voltage [V]	1.1	3.0
Rated Capacitance [F] at 25°C	32.1	100
Rated Capacitance [F] at 150°C	33.2	-
Initial ESR [mΩ] at 25°C	21.6	9.0
Initial ESR [mΩ] at 150 C	16.4	-
Maximum Operating Temperature [°C]	150	65
Minimum Operating Temperature [°C]	-40	-40
Cycle life at 25°C [no. of cycles]	>1,000,000	500,000

a cellulose separator, an aluminium current collector, and a quaternary salt solution as the electrolyte.

Each FastCap EC sample consists of two electrodes configured in a spirally wound double-layer fashion contained in a cylindrical cell—both made out of activated carbon, although traces of fluoride can be found in the electrode materials—an aluminium current collector, a polymer separator, and an ionic-based electrolyte. We hypothesize that the traces of fluoride in the electrode confirmed through energy-dispersive x-ray spectroscopy (EDX) analysis (see Figure 8) indicate that a fluoride-rich polymer chain has been used as the binding material.

III. EXPERIMENTAL DESIGN
A. ACCELERATED LIFE-CYCLE TESTING

The objective of the design of this experiment is to accelerate failure and investigate EC degradation at high-temperature values outside the manufacturer-defined operating envelope for EC used in onboard oil and gas drilling equipment. Note that data for LS Mtron is imported from [17]. Thus, we select five samples from the data available in [17] in order to eliminate cells cycled above the EC's surge voltage rating of 3V, as mentioned in Table 1. By eliminating the effect of high-charge cutoff voltage, we only investigate temperature-driven degradation at 80° C and 95° C. The selected samples underwent a constant current-constant voltage (CC-CV) charge profile followed by constant current (CC) discharge. For a summary of the accelerated test stress matrix, refer to Table 2. For a full description of the testing carried out on the LS Mtron samples, refer to [17].

TABLE 2. Accelerated lifecycle test matrix.

Cell no.	LS Mtron		FastCap	
	1, 2, 3	4, 5	1, 2	3, 4
Charge Profile	CC-CV	CC-CV	CC-CV	CC-CV
Charge current [A]	2	2	1	1
Charge cut-off voltage [V]	3	3	1	1
Time at CV [s]	600	600	600	600
Discharge current [A]	2	2	2	2
Temperature [°C]	80	95	160	200

Similar to the work in [17], the FastCap cells were cycled in a temperature-controlled chamber with a CC-CV charge profile followed by a CC discharge (see Figure 2). The current rate chosen for both charge and discharge is well below
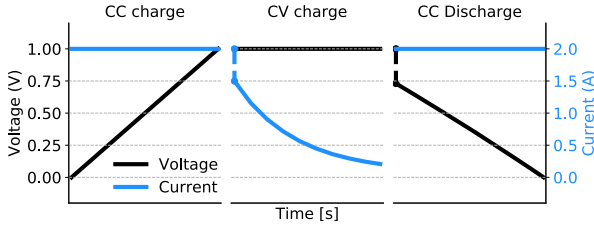
FIGURE 2. Charge-discharge profile: Constant current (CC) - constant voltage (CV) charge and constant current discharge.

the maximum rated discharge current (refer to Table 1) to minimise its effect on degradation. The FastCap samples have been cycled at temperatures of 160° C and 200° C, respectively. Additionally, in comparison to the LS Mtron samples cycled in [17] where all samples go up to surge voltage, FastCap cells' cutoff voltage does not exceed the rated voltage. We measure the survival time as number of cycles to EoL. The EoL criterion adopted here is a 30% decrease in capacitance.

Capacitance and equivalent series resistance (ESR) are measured periodically to monitor the degradation. Capacitance, C was computed by using the average of all instantaneous discharge capacitance measurements between 80% and 40% of the rated voltage. The instantaneous discharge capacitance was calculated at each time-step by:

$$C_{instantaneous} = \frac{I(t)dt}{dV(t)} \qquad (1)$$

where dt is the change in time, $I(t)$ is the instantaneous discharge current at time t, and $dV(t)$ is the change in discharge voltage at time t. ESR is determined by the intersection method described in [14] and [32]. In this method, the instantaneous drop in discharge voltage, V_1 and associated time t_1 are used as proxy to determine the constant slope of the discharge voltage curve with reference to the time at which the discharge began, with time and voltage denoted as t_0 and V_0. This method is illustrated in Figure 3 and explained in depth in [14], [32], whilst the equation used to determine the ESR is:

$$ESR = \frac{C(V_0 - V_1) + I(t_1 - t_0)}{IC} \qquad (2)$$

where C is the capacitance and I the discharge current.

B. ACCELERATED LIFE-CYCLE TESTING RESULTS

We summarise capacitance value measured at the first charge-discharge cycle in Table 3 and cycle value for EoL, and we illustrate the percentage of capacitance fade as a function of cycle numbers at all stress levels for each sample in Figure 4. Note: we define one cycle as one full charge/discharge at constant current. A decrease in capacitance to less than 70% of value measured at first cycle is observed in under 1,000 cycles for both capacitor models, with the exception of the FastCap cells 1 and 2 cycled at 160° C, which falls to just under 95% at 1,800 cycles. This indicates that when operated close to
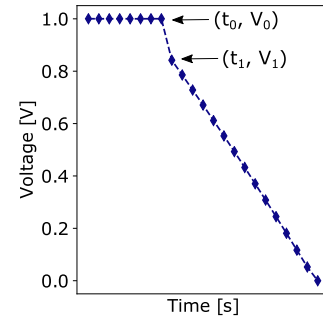
FIGURE 3. Voltage and time values used for calculation of capacitance and equivalent series resistance at each discharge.

TABLE 3. Capacitance and end of life measurements for all cells.

	Cell no.	Temp. [°C]	Capacitance[a] [F]	EoL cycle no.[b]
LS Mtron	1	80	101.09	900
	2	80	99.97	889
	3	80	100.65	783
	4	95	89.96	209
	5	95	89.3	213
FastCap	1	160	35.39	-
	2	160	35.05	-
	3	200	33.51	917
	4	200	33.26	876

[a] Measured during the first charge-discharge cycle,
[b] Measured as 30% decrease in capacitance calculated at first cycle.

the maximum manufacturer-recommended temperature envelope, the FastCap cell can withstand a relatively high number of cycles. The trend in capacitance value is generally nonmonotonic and does not always follow the traditional exponential curve, as indicated in literature [14], [17]. In particular, samples operating at more than 20° C above the manufacturer-specified temperature envelope (FastCAP cells at 200° C and LS Mtron cells at 110° C and 125° C) have a high degradation rate with a sudden acceleration in degradation once the cell reaches approximately 90% of initial capacitance value. The sudden change in degradation rate is termed the "knee" point in capacitance fade. The occurrence of the "knee" point is only observed in FastCap Cells 3 and 4, as illustrated in Figure 4. This is a common occurrence in lithium-ion batteries [28]; however, it is an understudied topic in EC literature.

EoL occurs first by reaching the 30% decrease in capacitance criteria threshold as opposed to the 100% increase in resistance for every sample included in this work. Based on the results obtained, the nonmonotonic degradation trend dependent on temperature is thus challenging to model with traditional exponential models previously employed for lithium-ion battery degradation estimation [19], [33]. In addition, such a mathematical model does not have the ability to estimate the uncertainty, generally captured in a CI, unless it is coupled with a particle filter [18], [33].
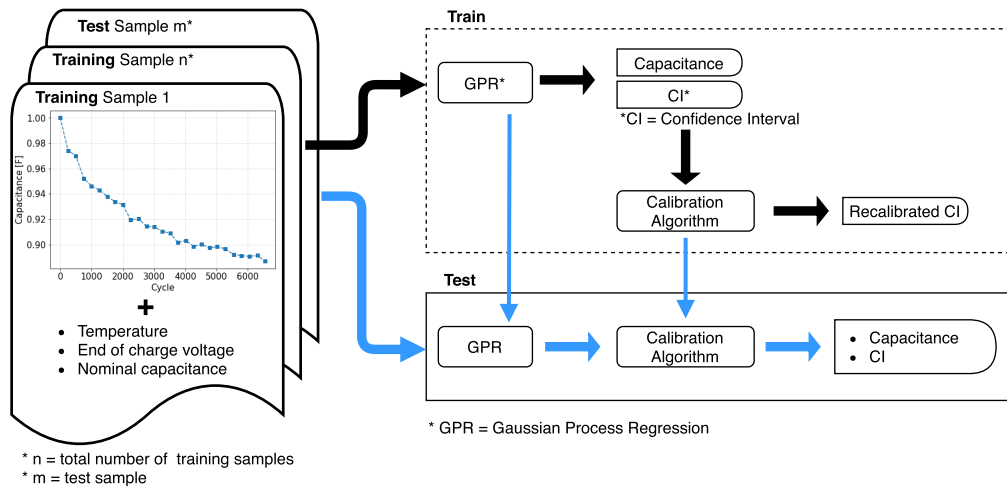
IV. MACHINE LEARNING DEGRADATION MODEL

Based on the accelerated life-cycle tests results, the end of life measured as 30% decrease in capacitance is reached first. We therefore focus on using capacitance as a proxy for modelling of the degradation. From a machine learning
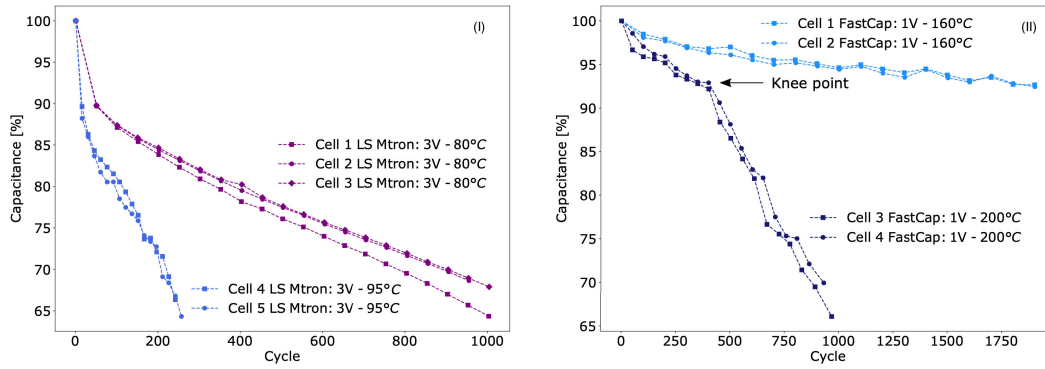
FIGURE 4. Capacitance degradation trend for all samples. (I) LS Mtron cells, (II) FastCap cells.

FIGURE 5. Schematic of train and test procedure of the Gaussian process algorithm (GPR).

perspective we treat modelling of the degradation as a supervised regression problem where we use four features as input to predict the degradation trend, measured as a percentage in capacitance fade when referenced to the first cycle. Formally, the model maps from a set of inputs, $\mathbf{x}$ to a set of outputs, $\mathbf{y}$. The labeled training set pairs are denoted here as $\mathcal{D} = (\mathbf{x}_i, \mathbf{y}_i)_{i=1}^{n_t}$, where n_t is the number of training samples. The four-feature input vector $\mathbf{x}$ consists of temperature, cut-off voltage, discharge current and cycle number as illustrated in Figure 5. The selected input variables capture the operational condition (quantified as temperature and end of charge voltage) as well as EC specific properties (nominal capacitance and degradation trend), and thus facilitate model generalisation to other cells irrespective of the degradation mechanism at other temperatures provided this information is available. Mathematically, the regression task is summarised by:

$$\mathbf{y} = f(\mathbf{x}) + \epsilon \qquad (3)$$

where ϵ is a Gaussian distributed noise contribution $\mathcal{N}(0, \sigma^2)$ and $f(\mathbf{x})$ represents the function that requires learning. To satisfy the uncertainty estimation requirement we employ a Bayesian-based algorithm to solve equation 3, namely

Gaussian process regression. Bayesian based algorithms including relevance vector machine (RVM) as formulated by Tipping [34] and Gaussian process regression (GPR) have been used for battery capacity estimation [24], [35]; however none have been used for EC capacitance fade degradation. We chose GPR as the primary algorithm due to its non-parametric properties and its ability to provide predictive distributions for test cases. Critically, as opposed to RVM where predictive uncertainties get smaller when moving away from the training cases [36], GPR does not suffer from such limitations. It is worth mentioning however, that this property comes at the expense of a slower computation. Given that the models are computed offline, however, this poses no concern in the present paper.

For a given set of training data, $\mathcal{D} = (\mathbf{x}_i, \mathbf{y}_i)_{i=1}^{n_t}$, there is an infinite number of functions that can potentially fit the data. A GPR simply assigns a probability to each of these functions. The mean of this probability distribution then represents the most probable characterization of the data. [37] Thus, a Gaussian process is completely specified by its mean function and covariance function. Formally the function in equation 3 can be summarised by:

$$f(\mathbf{x}) \sim \mathcal{GP}(m(\mathbf{x}), k(\mathbf{x}, \mathbf{x}')) \qquad (4)$$

where $m(\mathbf{x})$ is the mean and $k(\mathbf{x}, \mathbf{x}')$ is the covariance function. The mean and covariance are defined by:

$$m(\mathbf{x}) = \mathbb{E}[f(\mathbf{x})] \tag{5}$$

$$k(\mathbf{x}, \mathbf{x}') = \mathbb{E}[(f(\mathbf{x} - m(\mathbf{x}))(f(\mathbf{x}' - m(\mathbf{x}')))] \tag{6}$$

Given the formulation of GPR, the function $f(\mathbf{x})$ is a sample from a Gaussian process as defined in equation 4 and does not require learning the parameters of a regression function $f(\theta, \mathbf{x})$, where θ are the parameters, in a traditional sense. This makes GPR a non-parametric regression approach capable of modeling the nonlinear degradation trajectories seen in Figure 5. Commonly used covariance functions, also called kernels, include the squared exponential (SE), radial basis, or Mattérn [37]. For an in-depth analysis of popular kernels, we refer the reader to the work of Wilson and Adams [38], whilst a comprehensive presentation of Gaussian processes is undertaken in Rasmussen and Williams [37]. In this work, we adopt a rational quadratic (RQ) kernel in combination with a white noise (WN) kernel. The RQ kernel is defined by

$$k_{RQ}(\mathbf{x}, \mathbf{x}') = \left(1 + \frac{d(\mathbf{x}, \mathbf{x}')^2}{2\alpha l^2}\right)^{-\alpha} \tag{7}$$

where α is the scale mixture parameter, l is the length scale of the kernel, and $d(\cdot, \cdot)$ is the Euclidean distance. The RQ kernel is equivalent to adding together many SE kernels with different lengthscales, giving it a smooth output whilst also displaying long range trends [38]. Such properties are desired for modelling of the EC degradation trends summarised in Figure 4. The addition of the white noise in the kernel is motivated by a desire to model the sensor measurement and shift noise component of equation 3 and prevent overfitting of the data, a behaviour commonly encountered when GPR is fitted on small a dataset consisting of just five cells [39]. The WN kernel is defined by the addition of a constant to the diagonal of the covariance matrix and it is given by:

$$k_{WN}(\mathbf{x}, \mathbf{x}') = \begin{cases} \sigma_n^2, & x \equiv x' \\ 0, & \text{otherwise} \end{cases} \tag{8}$$

where σ_n^2 is the variance of observation noise, normally distributed with zero mean.

We then compute the kernel used in the model as a summation of the two kernels, RQ and WN kernel, as:

$$k(\mathbf{x}, \mathbf{x}') = k_{RQ}(\mathbf{x}, \mathbf{x}') + k_{WN}(\mathbf{x}, \mathbf{x}') \tag{9}$$

It is common practice to assume that the mean function is zero everywhere, since uncertainty about the mean function can be taken into account by adding an extra term to the kernel, and thus we adopt a similar approach [37]. To make predictions of a new vector, $\mathbf{x}^*$ containing the desired temperature, end of charge voltage, nominal capacitance value and cycle number, the algorithm computes the conditional distribution $p(\mathbf{y}^*|\mathbf{x}^*, \mathbf{x}, \mathbf{y})$. The conditional distribution can be analytically computed by:

$$p(\mathbf{y}^*|\mathbf{x}^*, \mathbf{x}, \mathbf{y}) = K(\mathbf{x}, \mathbf{x}^*)^T K(\mathbf{x}, \mathbf{x}^*)^{-1} \mathbf{y} \tag{10}$$

where the mean vector, m^* and the covariance matrix, Σ^* are defined by:

$$m^* = K(\mathbf{x}, \mathbf{x}^*)^T K(\mathbf{x}, \mathbf{x}^*)^{-1} \mathbf{y} \tag{11}$$

$$\Sigma^* = K(\mathbf{x}, \mathbf{x}^*) - K(\mathbf{x}, \mathbf{x}^*)^T K(\mathbf{x}, \mathbf{x}^*)^{-1} K(\mathbf{x}, \mathbf{x}^*) \tag{12}$$

The formulation in equation 10 thus suggests that the prediction is not only a point estimate, but also has built in uncertainty information as it is a one-dimensional Gaussian distribution. Therefore, each percentage of degradation in capacitance predicted is accompanied by a confidence interval (CI). We calculate the 95% CI using the predicted value, $\hat{\mathbf{y}}^*$ and the model predicted standard deviation, σ^* by:

$$CI = \hat{\mathbf{y}}^* \pm 2\sigma^* \tag{13}$$

The GPR model considered in this work uses the constrained limited memory BFGS method as the optimizer for maximizing the log-marginal-likelihood (LML) as proposed in [40] and implemented in scipy [41] and scikit-learn [42]. The LML may have multiple local minima, therefore the optimizer is initialised repeatedly to avoid such points, in our case we have selected 5 restarts. To improve accuracy and prevent overfitting of the GPR model, we perform hyper-parameter tuning using a random search approach, rather than a grid search. The random search approach is proven to be more efficient for hyper-parameter optimisation than trials on a grid [43], hence the adoption here. The two kernel parameters in equation 7, l and α, and the single parameter, σ_n^2, in equation 8, are all drawn from normal distributions and are determined with a random search cross-validation approach. We adopt a group cross validation approach where each fold is represented by one of the five training cells. This is done to maintain the temporal dependencies of degradation within each cell and thus prevent over-fitting of the regression algorithm.

Since the model output is a univariate Gaussian distribution with mean, $\hat{\mathbf{y}}^*$ and standard deviation σ^* we also want to determine how calibrated the model is. A calibrated model in a regression setting, means that the prediction should fall in a 95% CI (refer to equation 13 for CI definition) approximately 95% of the time. Thus, we first calculate calibration score (CS) based on a 95% CI in equation 13 using the formula:

$$CS_{2\sigma} = \frac{1}{N} \sum_{i=1}^{N} [|\hat{\mathbf{y}}_i^* - \mathbf{y}^*| < 2\sigma^*] \tag{14}$$

where $\hat{\mathbf{y}}^*$ is the predicted percentage change in capacitance, $\mathbf{y}^*$ is the label and N is the total number of cycles for the cell under scrutiny. Given a score outside a $\pm 1\%$ threshold of the 95% CS score, we perform a recalibration of the model. We recalibrate by fitting a regression model on the GPR predicted probability and expected probability. Typically, recalibration is done via isotonic regression [44]; however, this method fits a step-wise function prone to overfitting. For this reason, we replace the recalibration algorithm with a kernel ridge regression (KRR), an algorithm that is capable
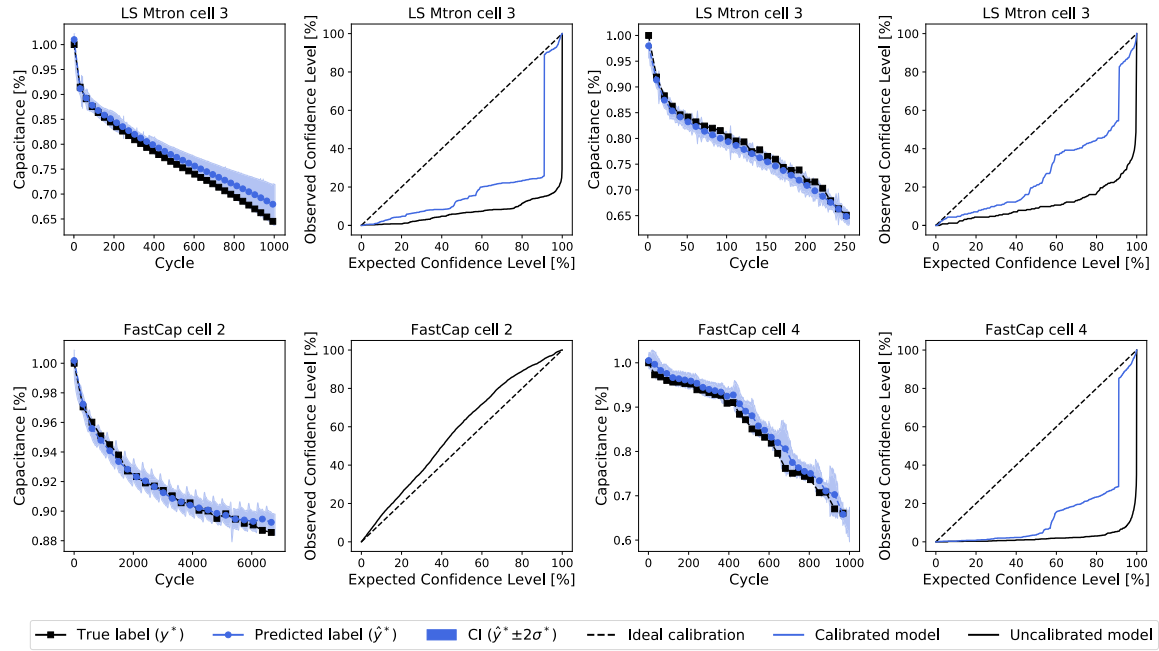
FIGURE 6. Predictions and calibration curves. (I) Prediction cell 5 LS Mtron, (II) Reliability plot cell 5 LS Mtron, (III) Prediction Cell 3 LS Mtron, (IV) Reliability plot cell 3 LS Mtron, (V) Prediction cell 4 FastCap, (VI) Reliability plot cell 4 FastCap, (VII) Prediction cell 2 FastCap, (VIII) Reliability plot cell 2 FastCap.

of mapping linear functions based on the non-linear function in the original input space introduced via the kernel. Since the recalibration algorithm can be replaced by most regression-based algorithms, we omit a detailed explanation of KRR in this work. For the interested reader, the KRR algorithm is presented in detail by Murphy in [29]. The KRR model employed for recalibration uses a radial basis kernel with a gamma value of 100. GPR accuracy is evaluated based on two metrics: mean absolute percent error (MAPE) (see equation 15) and root mean squared percent error (RMSPE) (equation 16). Because both MAPE and RMSPE are normalised measures of accuracy, they can be used to compare estimation performance across all cells irrespective of manufacturer, degradation trend, or nominal capacitance.

$$MAPE(\hat{y}_i^*, y_i^*) = \frac{1}{N} \sum_{i=1}^{N} \frac{|\hat{y}_i^* - y_i^*|}{y_i^*} \qquad (15)$$

$$RMSPE(\hat{y}_i^*, y_i^*) = \sqrt{\frac{1}{N} \sum_{i=1}^{N} \left(\frac{\hat{y}_i^* - y_i^*}{y_i^*} \right)^2} \qquad (16)$$

where, for both equations, $\hat{\mathbf{y}}^*$ is the predicted % change in capacitance, $\mathbf{y}^*$ is the measured % change in capacitance and N is the total number of cycles for the cell under scrutiny.

V. RESULTS

The accuracy of the GPR algorithm on each of the test cells measured as MAPE, RMSPE, and $CS_{2\sigma}$ is summarised in Table 4 and visualised in Figure 6. We also further

TABLE 4. Gaussian process results on test cells from both manufacturers, LS Mtron and FastCap.

	MAPE	RMSPE	$CS_{2\sigma}$ uncalibrated[c]	$CS_{2\sigma}$ calibrated[c]
Cell 3[a]	2.13	2.53	17	92
Cell 5[a]	1.21	1.38	32	89
Cell 2[b]	0.23	0.31	96	-
Cell 4[b]	1.91	2.3	1	92
Average	1.37	1.63	39	93

[a] LS Mtron cells, [b] FastCap cells, [c] All values in [%].

analyse the model uncertainty quantification by displaying the reliability diagnostics curves in Figure 6, similar to the work of Kuleshov et. al. in [45]. The reliability diagnostics curve displays the true frequency of points (true percent decrease in capacitance value) in each confidence interval relative to the estimated fraction of points (estimated percent decrease in capacitance value) in the interval. We divide each confidence interval in m confidence levels that are monotonically increasing on the interval [0, 1] i.e. $0 < p_1 < p_2 < \ldots < p_m < 1$, where m is the desired number of quantiles. We then compute the empirical probability for each threshold by counting the frequency of true labels in each confidence level p_m. The empirical distribution is thus calculated as:

$$\hat{p}_m = \frac{|y_i| f(x_i) \le p_m, \ i = 1, \ldots, N|}{N} \qquad (17)$$

where N is the number of cycles for a particular cell. Essentially, since the output is a Gaussian distribution, $\hat{p}_m$ denotes the fraction of the data for which y_i lies below the

p-th quantile calculated as $y_i^* + z_m \cdot \sigma^*$, where z_m is the z-value for the desired quantile.

Therefore, to visualise calibration for results analysis purposes, we plot the observed confidence versus expected confidence, i.e. $(p_m, \hat{p}_m)$ and obtain the reliability plots in Figure 6. An ideal calibration is represented by a dotted line, meaning $p_m = \hat{p}_m$. With the exception of FastCap cell 2, which exhibits a near ideal reliability plot, all other cells required calibration of the output. Despite the fact that the reliability curve greatly improves after model recalibration when evaluated at a confidence value greater than 90%, the reliability plot shows poor behaviour at lower confidence values, although the calibration score greatly improves when the two reliability curves of calibrated and uncalibrated models are compared. The lowest error is achieved on FastCap cell 2, whilst the highest error is obtained on LS Mtron cell 3. The reason for the error increase is caused by a higher deviation of the degradation trend of the test cell, LS Mtron cell 3, from the two training cells 1 and 2, respectively (refer to Figure 4). Such deviation is caused by cell intrinsic material composition variation introduced during the manufacturing process. The model captures the increase in error caused by such deviation from training data by increasing the standard deviation value (the blue shaded area in Figure 6) around the predicted mean, a behaviour that is desired when the model is uncertain in its prediction.

VI. DISCUSSIONS

The accelerated life-cycle testing coupled with the modelling approach presented in this paper offers the potential for manufacturers to accelerate testing and reduce time for product qualification. Machine learning models can predict degradation as a function of the number of cycles together with a CI for cells operated at various temperatures outside the manufacturer-recommended operating envelope.

Additionally, at the prototyping stage, the model can be trained on available temperature cycling data and estimate degradation at other temperatures, reducing test time, speeding up the design process, and cutting costs. The model can also be used to generate synthetic data where only a limited number of cycles is available. For example, when there is missing characterisation data, the model can estimate degradation in between characterisation tests for a particular EC design operated at a fixed temperature.

Finally, the model can also be used for prognostics and health management purposes by predicting remaining useful life at a constant temperature and constant end of charge value. Therefore, given an input sequence of cycles as well as associated temperature and end of charge voltage, the model can predict degradation together with a CI until the EoL threshold is reached.

VII. CONCLUSION

EC reliability is important when operating in extreme temperature environments, as in the case of downhole drilling equipment for geothermal or oil and gas exploration.
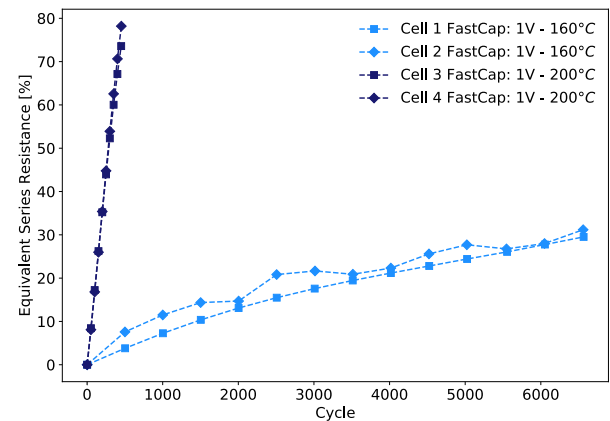

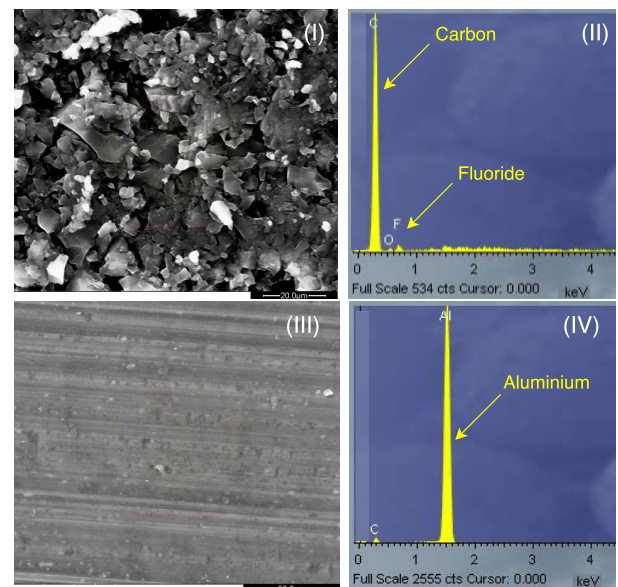**FIGURE 7.** Resistance degradation trend FastCap cells.

FIGURE 8. FastCap sample analysis. (I) Scanning electron microscopy (SEM) of carbon electrode, (II) EDX spectrum of carbon electrode, (III) SEM of aluminium current collector and (III) EDX spectrum of aluminium current collector.

Therefore, our research focused on addressing the knowledge gaps in modelling the effects of temperature on EC EoL when the devices are operated outside the manufacturer-specified temperature rating. This paper incorporated a machine learning algorithm, GPR, as a technique for modelling the capacitance fade of ECs and qualified the uncertainty in the associated predictions. GPR was trained on data obtained from accelerated life-cycle testing of two commercially available manufacturers under various temperatures ranging from 80° C to 200° C.

The experimental work concluded that all samples reached the 30% decrease in capacitance EoL threshold first. For this reason, capacitance fade was used as a proxy for degradation. The accelerated life-cycle data was then used as input to the GPR algorithm to model the degradation. The model used four features as input: temperature, end of charge voltage, nominal capacitance value, and cycle number. It used one

target variable: percentage decrease in capacitance. GPR has shown an average root mean squared error of 2% and a mean calibration score of 93% when referenced to a 95% CI. We propose that our model can be used for the qualification of ECs at a range of operating temperatures, providing accurate insight into the EC capacitance degradation curve as a function of charge-discharge cycles. Our future research will expand on EC types and accelerated life-cycle test parameters.

.

APPENDIX A
See Figures 7 and 8.

REFERENCES

[1] H. Chloe, G. Tim, R. Chris, and P. Temma, "Global energy storage market forecast 2019," Lux Res., New York, NY, USA, Tech. Rep., 2019.

[2] I. Antonopoulos, V. Robu, B. Couraud, D. Kirli, S. Norbu, A. Kiprakis, D. Flynn, S. Elizondo-Gonzalez, and S. Wattam, "Artificial intelligence and machine learning approaches to energy demand-side response: A systematic review," *Renew. Sustain. Energy Rev.*, vol. 130, Sep. 2020, Art. no. 109899.

[3] M. Andoni, V. Robu, W.-G. Fruh, and D. Flynn, "Strategic decision-making for power network investments with distributed renewable generation," in *Proc. 19th Int. Conf. Auto. Agents MultiAgent Syst.*, 2020, pp. 52–60.

[4] O. Schmidt, A. Hawkes, A. Gambhir, and I. Staffell, "The future cost of electrical energy storage based on experience rates," *Nature Energy*, vol. 2, no. 8, pp. 1–8, Aug. 2017.

[5] H. J. Schellnhuber, S. Rahmstorf, and R. Winkelmann, "Why the right climate target was agreed in Paris," *Nature Climate Change*, vol. 6, no. 7, pp. 649–653, Jul. 2016.

[6] *Renewable Energy: A Key Climate Solutions*, IRENA, Abu Dhabi, United Arab Emirates, 2017.

[7] *Global Renewables Outlook: Energy Transformation 2050*, IRENA, Abu Dhabi, United Arab Emirates, 2020.

[8] R. Signorelli and J. Cooley, "Energy storage and generation for extreme temperature and pressure and directional measurement while drilling applications," FastCAP Syst. Corp., Boston, MA, USA, Tech. Rep. DOE-FAST-05503, 2015.

[9] K. B. Chin, E. J. Brandon, R. V. Bugga, M. C. Smart, S. C. Jones, F. C. Krause, W. C. West, and G. G. Bolotin, "Energy storage technologies for small satellite applications," *Proc. IEEE*, vol. 106, no. 3, pp. 419–428, Mar. 2018.

[10] R. V. Bugga and E. J. Brandon, "Energy storage for the next generation of robotic space exploration," *Electrochem. Soc. Interface*, vol. 29, no. 1, p. 59, 2020.

[11] L. Kirschbaum, D. Roman, G. Singh, J. Bruns, V. Robu, and D. Flynn, "AI-driven maintenance support for downhole tools and electronics operated in dynamic drilling environments," *IEEE Access*, vol. 8, pp. 78683–78701, 2020.

[12] S. Ishimoto, Y. Asakawa, M. Shinya, and K. Naoi, "Degradation responses of Activated-Carbon-Based EDLCs for higher voltage operation and their factors," *J. Electrochem. Soc.*, vol. 156, no. 7, p. A563, 2009.

[13] B. K. Kim, S. Sy, A. Yu, and J. Zhang, "Electrochemical supercapacitors for energy storage and conversion," in *Handbook of Clean Energy Systems*. Hoboken, NJ, USA: Wiley, 2015, pp. 1–25.

[14] H. Gualous, R. Gallay, G. Alcicek, B. Tala-Ighil, A. Oukaour, B. Boudart, and P. Makany, "Supercapacitor ageing at constant temperature and constant voltage and thermal shock," *Microelectron. Rel.*, vol. 50, nos. 9–11, pp. 1783–1788, Sep. 2010.

[15] K. Fic, M. He, E. J. Berg, P. Novák, and E. Frackowiak, "Comparative operando study of degradation mechanisms in carbon-based electrochemical capacitors with Li$_2$SO$_4$ and LiNO$_3$ electrolytes," *Carbon*, vol. 120, pp. 281–293, Aug. 2017.

[16] A. M. Engstrom and F. M. Doyle, "Exploring the cycle behavior of electrodeposited vanadium oxide electrochemical capacitor electrodes in various aqueous environments," *J. Power Sources*, vol. 228, pp. 120–131, Apr. 2013.

[17] N. Williard, D. Baek, J. W. Park, B.-O. Choi, M. Osterman, and M. Pecht, "A life model for supercapacitors," *IEEE Trans. Device Mater. Rel.*, vol. 15, no. 4, pp. 519–528, Dec. 2015.

[18] F. Yang, D. Wang, Y. Xing, and K.-L. Tsui, "Prognostics of Li(NiMnCo)O$_2$-based lithium-ion batteries using a novel battery degradation model," *Microelectron. Rel.*, vol. 70, pp. 70–78, Mar. 2017.

[19] B. Xu, A. Oudalov, A. Ulbig, G. Andersson, and D. S. Kirschen, "Modeling of lithium-ion battery degradation for cell life assessment," *IEEE Trans. Smart Grid*, vol. 9, no. 2, pp. 1131–1140, Mar. 2018.

[20] A. Stetco, F. Dinmohammadi, X. Zhao, V. Robu, D. Flynn, M. Barnes, J. Keane, and G. Nenadic, "Machine learning methods for wind turbine condition monitoring: A review," *Renew. Energy*, vol. 133, pp. 620–635, Apr. 2019.

[21] Y. Zhou, Y. Huang, J. Pang, and K. Wang, "Remaining useful life prediction for supercapacitor based on long short-term memory neural network," *J. Power Sources*, vol. 440, Nov. 2019, Art. no. 227149.

[22] Y. Zhou, Y. Wang, K. Wang, L. Kang, F. Peng, L. Wang, and J. Pang, "Hybrid genetic algorithm method for efficient and robust evaluation of remaining useful life of supercapacitors," *Appl. Energy*, vol. 260, Feb. 2020, Art. no. 114169.

[23] A. Soualhi, A. Sari, H. Razik, P. Venet, G. Clerc, R. German, O. Briat, and J. M. Vinassa, "Supercapacitors ageing prediction by neural networks," in *Proc. IECON-39th Annu. Conf. IEEE Ind. Electron. Soc.*, Nov. 2013, pp. 6812–6818.

[24] R. R. Richardson, M. A. Osborne, and D. A. Howey, "Gaussian process regression for forecasting battery state of health," *J. Power Sources*, vol. 357, pp. 209–219, Jul. 2017.

[25] K. Liu, Y. Shang, Q. Ouyang, and W. D. Widanage, "A data-driven approach with uncertainty quantification for predicting future capacities and remaining useful life of lithium-ion battery," *IEEE Trans. Ind. Electron.*, vol. 68, no. 4, pp. 3170–3180, Apr. 2021.

[26] K. Liu, X. Hu, Z. Wei, Y. Li, and Y. Jiang, "Modified Gaussian process regression models for cyclic capacity prediction of lithium-ion batteries," *IEEE Trans. Transport. Electrific.*, vol. 5, no. 4, pp. 1225–1236, Dec. 2019.

[27] P. Tagade, K. S. Hariharan, S. Ramachandran, A. Khandelwal, A. Naha, S. M. Kolake, and S. H. Han, "Deep Gaussian process regression for lithium-ion battery health prognosis and degradation mode diagnosis," *J. Power Sources*, vol. 445, Jan. 2020, Art. no. 227281.

[28] W. Diao, S. Saxena, B. Han, and M. Pecht, "Algorithm to determine the knee point on capacity fade curves of lithium-ion cells," *Energies*, vol. 12, no. 15, p. 2910, Jul. 2019.

[29] K. P. Murphy, *Machine Learning: A Probabilistic Perspective*. Cambridge, MA, USA: MIT Press, 2012.

[30] Y. Gao, "Graphene and polymer composites for supercapacitor applications: A review," *Nanosc. Res. Lett.*, vol. 12, no. 1, p. 387, Dec. 2017.

[31] J. Yan, Q. Wang, T. Wei, and Z. Fan, "Recent advances in design and fabrication of electrochemical supercapacitors with high energy densities," *Adv. Energy Mater.*, vol. 4, no. 4, Mar. 2014, Art. no. 1300816.

[32] M. Uno and K. Tanaka, "Accelerated charge–discharge cycling test and cycle life prediction model for supercapacitors in alternative battery applications," *IEEE Trans. Ind. Electron.*, vol. 59, no. 12, pp. 4704–4712, Dec. 2012.

[33] L. Zhang, Z. Mu, and C. Sun, "Remaining useful life prediction for lithium-ion batteries based on exponential model and particle filter," *IEEE Access*, vol. 6, pp. 17729–17740, 2018.

[34] M. E. Tipping, "Sparse Bayesian learning and the relevance vector machine," *J. Mach. Learn. Res.*, vol. 1, pp. 211–244, Sep. 2001.

[35] D. Roman, R. Dickie, V. Robu, and D. Flynn, "A review of the role of prognostics in predicting the remaining useful life of assets," *Saf. Rel.-Theory Appl.*, vol. 135, pp. 1–9, Jun. 2017.

[36] C. E. Rasmussen and J. Quiñonero-Candela, "Healing the relevance vector machine through augmentation," in *Proc. 22nd Int. Conf. Mach. Learn. (ICML)*, 2005, pp. 689–696.

[37] C. E. Rasmussen and C. Williams, *Gaussian Processes for Machine Learning*, vol. 1. Cambridge, MA, USA: MIT Press, 2006, pp. 40–43.

[38] A. Wilson and R. Adams, "Gaussian process kernels for pattern discovery and extrapolation," in *Proc. Int. Conf. Mach. Learn.*, 2013, pp. 1067–1075.

[39] R. O. Mohammed and G. C. Cawley, "Over-fitting in model selection with Gaussian process regression," in *Proc. Int. Conf. Mach. Learn. Data Mining Pattern Recognit.* New York, NY, USA: Springer, 2017, pp. 192–205.

[40] R. H. Byrd, P. Lu, J. Nocedal, and C. Zhu, "A limited memory algorithm for bound constrained optimization," *SIAM J. Sci. Comput.*, vol. 16, no. 5, pp. 1190–1208, Sep. 1995.

[41] P. Virtanen *et al.*, "SciPy 1.0: Fundamental algorithms for scientific computing in Python," *Nature Methods*, vol. 17, pp. 261–272, Feb. 2020.

[42] F. Pedregosa, G. Varoquaux, A. Gramfort, V. Michel, B. Thirion, O. Grisel, M. Blondel, P. Prettenhofer, J. Vanderplas, R. Weiss, V. Dubourg, A. Passos, D. Cournapeau, M. Brucher, M. Perrot, and E. Duchesnay, "Scikit-learn: Machine learning in Python," *J. Mach. Learn. Res.*, vol. 12, no. 85, pp. 2825–2830, 2011. [Online]. Available: http://jmlr.org/papers/v12/pedregosa11a.html

[43] J. Bergstra and Y. Bengio, "Random search for hyper-parameter optimization," *J. Mach. Learn. Res.*, vol. 13, pp. 281–305, Feb. 2012.

[44] A. Niculescu-Mizil and R. Caruana, "Obtaining calibrated probabilities from boosting," in *Proc. UAI*, 2005, p. 413.

[45] V. Kuleshov, N. Fenner, and S. Ermon, "Accurate uncertainties for deep learning using calibrated regression," 2018, *arXiv:1807.00263*. [Online]. Available: http://arxiv.org/abs/1807.00263

DARIUS ROMAN received the M.Eng. degree (Hons.) in mechanical and electrical engineering from the University of Aberdeen. He is currently pursuing the Ph.D. degree in prognostics and health management for energy storage devices as part of CDT in embedded intelligence with Heriot-Watt University, Edinburgh. He had been working as a Design Verification Engineer in the Oil and gas industry, where he was responsible for FEA analysis and stress analysis of drilling equipment. His Ph.D. research project aims at using machine learning algorithms for state of health estimation and degradation prediction of lithium-ion batteries and electrochemical capacitors.

SAURABH SAXENA received the B.Tech. degree in electrical engineering from the Indian Institute of Technology (Banaras Hindu University), Varanasi, India, in 2011, and the Ph.D. degree in mechanical engineering from the University of Maryland, College Park, MD, USA, in 2020. He worked as a Project Assistant with the Indian Institute of Science Bangalore, India, on the modeling of lithium-ion batteries and supercapacitors. He is currently a Postdoctoral Researcher with the Applied Materials Division, Argonne National Laboratory, USA. He has been involved in various battery research projects for the last seven years. His research interests include accelerated testing and modeling, failure analysis, reliability, safety, and artificial intelligence enabled health management of lithium-ion batteries.

JENS BRUNS received the Dipl.-Ing. and Ph.D. degrees in mechanical engineering from the University of Hannover, Germany, in 1997 and 2003, respectively. He has work experience in nonlinear dynamics, numerical simulation, signal processing, and data analysis. Application areas include turbine blade dynamics, drilling fluid hydraulics, and mud-pulse telemetry. He has 17 years of work experience in the Oil and Gas industry. He is currently leading diagnostic and prognostic development work for drilling equipment with Baker Hughes, Celle, Germany.

ROBU VALENTIN received the Ph.D. degree with CWI, The Netherlands National Research Institute for Mathematics and Computer Science, Amsterdam, The Netherlands. He was a Senior Research Fellow with the University of Southampton, U.K., and a Visiting Scholar with the Computer Science Department, Harvard University, USA. He is currently an Associate Professor with Heriot-Watt University, Edinburgh, Scotland, U.K., where he is also the Co-Director of the Smart Systems Research Group. He is also a Research Affiliate with the Centre for Collective Intelligence, Massachusetts Institute of Technology (MIT), USA. He is also a Co-Investigator in several large-scale energy and AI-related projects, such as the National Centre for Energy Systems Integration, U.K., (CESI), the Offshore Robotics for Certification of Assets Hub (ORCA Hub), the Community-Scale Energy Demand Reduction in India (CEDRI) or the Responsive Energy Flexibility demonstration project in Orkney Islands (Reflex). He is also a Principal Investigator and an Academic Lead of the Knowledge Transfer Partnership (KTP) project Network Constraints Early Warning Systems (NCEWS) with SP Energy Networks. He has published more than 80 articles in top-ranked journals, conferences, and edited volumes, in both the areas of artificial intelligence and electrical engineering.
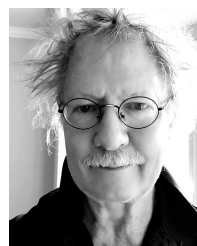
MICHAEL PECHT (Life Fellow, IEEE) received the B.S. degree in physics, the M.S. degree in electrical engineering, and the M.S. and Ph.D. degrees in engineering mechanics from the University of Wisconsin. He is currently a Professional Engineer. He is also the Director of the Center for Advanced Life Cycle Engineering (CALCE), University of Maryland (UMd), which is funded by over 150 of the world's leading electronics companies at more than US$6M/year. He is also a Professor of applied mathematics with UMd. He has 30,000+ citations, 80+ H-index. He is a PHM Society Life Fellow, an ASME Fellow, an ASM Fellow, an SAE Fellow, and an IMAPS Fellow. He received the highest reliability honor, the IEEE Reliability Society's Lifetime Achievement Award, in 2008, and the IEEE Exceptional Technical Achievement Award, in 2010, for his innovations in the area of prognostics and systems health management. He served as the Editor-in-Chief of IEEE Access for a period of six years, the IEEE TRANSACTIONS ON RELIABILITY for a period of nine years, *Microelectronics Reliability* for a period of 16 years. He is an Editor of *Circuit World*. He has also served on three U.S. National Academy of Science studies, two U.S. Congressional investigations in automotive safety, and as an expert to the U.S. FDA.

DAVID FLYNN (Member, IEEE) received the B.Eng. degree (Hons.) in electrical and electronic engineering, the M.Sc. degree (Hons.) in microsystems, and the Ph.D. degree in microscale magnetic components from Heriot-Watt University, Edinburgh, in 2002, 2003, and 2007, respectively. He is currently a Professor of smart systems with Heriot-Watt University, where he is also the Founder of the Smart Systems Group (SSG). The activities of the SSG involve multi-disciplinary expertise in sensor technologies, data analysis and systems engineering, to create predictive, and prescriptive analysis of systems. He is the Vice-Chair of the Institute of Engineering and Technology (IET) Scotland. He is also an IET Scholar as the recipient of (IET) Leslie H Paddle Prize. He also teaches Smart System Integration, Electrical Engineering, and Energy Systems.

• • •